



ASTRO-H Space X-ray Observatory White Paper

Chemical Evolution in High- z Universe

M. S. Tashiro (Saitama University), D. Yonetoku (Kanazawa University), M. Ohno (Hiroshima University), H. Sameshima (JAXA), H. Seta (Saitama University), H. Ueno (Saitama University), T. Nakagawa (JAXA), T. Tamura (JAXA), F. Paerels (Columbia University), N. Kawai (Tokyo Institute of Technology),
on behalf of the ASTRO-H Science Working Group

Abstract

In this paper, we demonstrate *ASTRO-H*'s capability to measure the chemical evolution in the high- z ($z \lesssim 3$) universe by observing X-ray afterglows of gamma-ray bursts (GRBs) and distant Blazars. Utilizing these sources as background light sources, the excellent energy resolution of *ASTRO-H/SXS* allows us to detect emission and absorption features from heavy elements in the circumstellar material in the host galaxies, from the intergalactic medium (IGM) and in the ejecta of GRB explosions. In particular, we can constrain the existence of the warm-hot intergalactic material (WHIM), thought to contain most of the baryons at redshift of $z \lesssim 3$, with a typical exposure of one day for a follow-up observation of a GRB afterglow or 300 ks exposure for several distant Blazars. In addition to the chemical evolution study, the combination of the SGD, HXI, SXI and SXS will measure, for the first time, the temporal behavior of the spectral continuum of GRB afterglows and Blazars over a broad energy range and short time scales allowing detailed modeling of jets. The ability to obtain these data from GRB afterglows will depend critically on the availability of GRB triggers and the capability of *ASTRO-H* to respond rapidly to targets of opportunity. At the present time it seems as if *Swift* will still be functioning normally during the first two years of *ASTRO-H* operations providing the needed triggering capability.

Complete list of the ASTRO-H Science Working Group

Tadayuki Takahashi^a, Kazuhisa Mitsuda^a, Richard Kelley^b, Felix Aharonian^c, Hiroki Akamatsu^d, Fumie Akimoto^e, Steve Allen^f, Naohisa Anabuki^g, Lorella Angelini^b, Keith Arnaud^b, Marc Audardⁱ, Hisamitsu Awaki^j, Aya Bamba^k, Marshall Bautz^l, Roger Blandford^f, Laura Brenneman^b, Greg Brown^m, Edward Cackettⁿ, Maria Chernyakova^c, Meng Chiao^b, Paolo Coppi^o, Elisa Costantini^d, Jelle de Plaa^d, Jan-Willem den Herder^d, Chris Done^p, Tadayasu Dotani^a, Ken Ebisawa^a, Megan Eckart^b, Teruaki Enoto^q, Yuichiro Ezoe^r, Andrew Fabianⁿ, Carlo Ferrignoⁱ, Adam Foster^s, Ryuichi Fujimoto^t, Yasushi Fukazawa^u, Stefan Funk^f, Akihiro Furuzawa^e, Massimiliano Galeazzi^v, Luigi Gallo^w, Poshak Gandhi^p, Matteo Guainazzi^x, Yoshito Haba^y, Kenji Hamaguchi^h, Isamu Hatsukade^z, Takayuki Hayashi^a, Katsuhiro Hayashi^a, Kiyoshi Hayashida^g, Junko Hiraga^{aa}, Ann Hornschemeier^b, Akio Hoshino^{ab}, John Hughes^{ac}, Una Hwang^{ad}, Ryo Iizuka^a, Yoshiyuki Inoue^a, Hajime Inoue^a, Kazunori Ishibashi^e, Manabu Ishida^a, Kumi Ishikawa^q, Yoshitaka Ishisaki^f, Masayuki Ito^{ae}, Naoko Iyomoto^{af}, Jelle Kaastra^d, Timothy Kallman^b, Tuneyoshi Kamae^f, Jun Kataoka^{ag}, Satoru Katsuda^a, Junichiro Katsuta^u, Madoka Kawaharada^a, Nobuyuki Kawai^{ah}, Dmitry Khangulyan^a, Caroline Kilbourne^b, Masashi Kimura^{ai}, Shunji Kitamoto^{ab}, Tetsu Kitayama^{aj}, Takayoshi Kohmura^{ak}, Motohide Kokubun^a, Saori Konami^r, Katsuji Koyama^{al}, Hans Krimm^b, Aya Kubota^{am}, Hideyo Kunieda^e, Stephanie LaMassa^o, Philippe Laurent^{an}, François Lebrun^{an}, Maurice Leutenegger^b, Olivier Limousin^{an}, Michael Loewenstein^b, Knox Long^{ao}, David Lumb^{ap}, Grzegorz Madejski^f, Yoshitomo Maeda^a, Kazuo Makishima^{aa}, Maxim Markevitch^b, Hironori Matsumoto^e, Kyoko Matsushita^{aq}, Dan McCammon^{af}, Brian McNamara^{as}, Jon Miller^{at}, Eric Miller^l, Shin Mineshige^{au}, Ikuyuki Mitsuishi^e, Takuya Miyazawa^e, Tsunefumi Mizuno^u, Koji Mori^z, Hideyuki Mori^e, Koji Mukai^b, Hiroshi Murakami^{av}, Toshio Murakami^t, Richard Mushotzky^h, Ryo Nagino^g, Takao Nakagawa^a, Hiroshi Nakajima^g, Takeshi Nakamori^{aw}, Shinya Nakashima^a, Kazuhiro Nakazawa^{aa}, Masayoshi Nobukawa^{al}, Hirofumi Noda^q, Masaharu Nomachi^{ax}, Steve O' Dell^{ay}, Hirokazu Odaka^a, Takaya Ohashi^r, Masanori Ohno^u, Takashi Okajima^b, Naomi Ota^{az}, Masanobu Ozaki^a, Frits Paerels^{ba}, Stéphane Paltaniⁱ, Arvind Parmar^x, Robert Petre^b, Ciro Pintoⁿ, Martin Pohlⁱ, F. Scott Porter^b, Katja Pottschmidt^b, Brian Ramsey^{ay}, Rubens Reis^{at}, Christopher Reynolds^h, Claudio Ricci^{au}, Helen Russellⁿ, Samar Safi-Harb^{bb}, Shinya Saito^a, Hiroaki Sameshima^a, Goro Sato^{ag}, Kosuke Sato^{aq}, Rie Sato^a, Makoto Sawada^k, Peter Serlemitsos^b, Hiromi Seta^{bc}, Aurora Simionescu^a, Randall Smith^s, Yang Soong^b, Łukasz Stawarz^a, Yasuharu Sugawara^{bd}, Satoshi Sugita^j, Andrew Szymkowiak^o, Hiroyasu Tajima^e, Hiromitsu Takahashi^u, Hiroaki Takahashi^g, Yoh Takei^a, Toru Tamagawa^q, Takayuki Tamura^a, Keisuke Tamura^e, Takaaki Tanaka^{al}, Yasuo Tanaka^a, Yasuyuki Tanaka^u, Makoto Tashiro^{bc}, Yuzuru Tawara^e, Yukikatsu Terada^{bc}, Yuichi Terashima^j, Francesco Tombesi^b, Hiroshi Tomida^{ai}, Yohko Tsuboi^{bd}, Masahiro Tsujimoto^a, Hiroshi Tsunemi^g, Takeshi Tsuru^{al}, Hiroyuki Uchida^{al}, Yasunobu Uchiyama^{ab}, Hideki Uchiyama^{be}, Yoshihiro Ueda^{au}, Shutaro Ueda^g, Shiro Ueno^{ai}, Shinichiro Uno^{bf}, Meg Urry^o, Eugenio Ursino^v, Cor de Vries^d, Shin Watanabe^a, Norbert Werner^f, Dan Wilkins^w, Shinya Yamada^r, Hiroya Yamaguchi^b, Kazutaka Yamaoka^e, Noriko Yamasaki^a, Makoto Yamauchi^z, Shigeo Yamauchi^{az}, Tahir Yaqoob^b, Yoichi Yatsu^{ah}, Daisuke Yonetoku^t, Atsumasa Yoshida^k, Takayuki Yuasa^q, Irina Zhuravleva^f, Abderahmen Zoghbi^h, and John ZuHone^b

^aInstitute of Space and Astronautical Science (ISAS), Japan Aerospace Exploration Agency (JAXA), Kanagawa 252-5210, Japan

^bNASA/Goddard Space Flight Center, MD 20771, USA

^cAstronomy and Astrophysics Section, Dublin Institute for Advanced Studies, Dublin 2, Ireland

^dSRON Netherlands Institute for Space Research, Utrecht, The Netherlands

^eDepartment of Physics, Nagoya University, Aichi 338-8570, Japan

^fKavli Institute for Particle Astrophysics and Cosmology, Stanford University, CA 94305, USA

^gDepartment of Earth and Space Science, Osaka University, Osaka 560-0043, Japan

^hDepartment of Astronomy, University of Maryland, MD 20742, USA

ⁱUniversité de Genève, Genève 4, Switzerland

^jDepartment of Physics, Ehime University, Ehime 790-8577, Japan

^kDepartment of Physics and Mathematics, Aoyama Gakuin University, Kanagawa 229-8558, Japan

^lKavli Institute for Astrophysics and Space Research, Massachusetts Institute of Technology, MA 02139, USA

^mLawrence Livermore National Laboratory, CA 94550, USA

ⁿInstitute of Astronomy, Cambridge University, CB3 0HA, UK

^oYale Center for Astronomy and Astrophysics, Yale University, CT 06520-8121, USA

^pDepartment of Physics, University of Durham, DH1 3LE, UK

^qRIKEN, Saitama 351-0198, Japan

^rDepartment of Physics, Tokyo Metropolitan University, Tokyo 192-0397, Japan

^sHarvard-Smithsonian Center for Astrophysics, MA 02138, USA

- ^tFaculty of Mathematics and Physics, Kanazawa University, Ishikawa 920-1192, Japan
- ^uDepartment of Physical Science, Hiroshima University, Hiroshima 739-8526, Japan
- ^vPhysics Department, University of Miami, FL 33124, USA
- ^wDepartment of Astronomy and Physics, Saint Mary's University, Nova Scotia B3H 3C3, Canada
- ^xEuropean Space Agency (ESA), European Space Astronomy Centre (ESAC), Madrid, Spain
- ^yDepartment of Physics and Astronomy, Aichi University of Education, Aichi 448-8543, Japan
- ^zDepartment of Applied Physics, University of Miyazaki, Miyazaki 889-2192, Japan
- ^{aa}Department of Physics, University of Tokyo, Tokyo 113-0033, Japan
- ^{ab}Department of Physics, Rikkyo University, Tokyo 171-8501, Japan
- ^{ac}Department of Physics and Astronomy, Rutgers University, NJ 08854-8019, USA
- ^{ad}Department of Physics and Astronomy, Johns Hopkins University, MD 21218, USA
- ^{ae}Faculty of Human Development, Kobe University, Hyogo 657-8501, Japan
- ^{af}Kyushu University, Fukuoka 819-0395, Japan
- ^{ag}Research Institute for Science and Engineering, Waseda University, Tokyo 169-8555, Japan
- ^{ah}Department of Physics, Tokyo Institute of Technology, Tokyo 152-8551, Japan
- ^{ai}Tsukuba Space Center (TKSC), Japan Aerospace Exploration Agency (JAXA), Ibaraki 305-8505, Japan
- ^{aj}Department of Physics, Toho University, Chiba 274-8510, Japan
- ^{ak}Department of Physics, Tokyo University of Science, Chiba 278-8510, Japan
- ^{al}Department of Physics, Kyoto University, Kyoto 606-8502, Japan
- ^{am}Department of Electronic Information Systems, Shibaura Institute of Technology, Saitama 337-8570, Japan
- ^{an}IRFU/Service d'Astrophysique, CEA Saclay, 91191 Gif-sur-Yvette Cedex, France
- ^{ao}Space Telescope Science Institute, MD 21218, USA
- ^{ap}European Space Agency (ESA), European Space Research and Technology Centre (ESTEC), 2200 AG Noordwijk, The Netherlands
- ^{aq}Department of Physics, Tokyo University of Science, Tokyo 162-8601, Japan
- ^{ar}Department of Physics, University of Wisconsin, WI 53706, USA
- ^{as}University of Waterloo, Ontario N2L 3G1, Canada
- ^{at}Department of Astronomy, University of Michigan, MI 48109, USA
- ^{au}Department of Astronomy, Kyoto University, Kyoto 606-8502, Japan
- ^{av}Department of Information Science, Faculty of Liberal Arts, Tohoku Gakuin University, Miyagi 981-3193, Japan
- ^{aw}Department of Physics, Faculty of Science, Yamagata University, Yamagata 990-8560, Japan
- ^{ax}Laboratory of Nuclear Studies, Osaka University, Osaka 560-0043, Japan
- ^{ay}NASA/Marshall Space Flight Center, AL 35812, USA
- ^{az}Department of Physics, Faculty of Science, Nara Women's University, Nara 630-8506, Japan
- ^{ba}Department of Astronomy, Columbia University, NY 10027, USA
- ^{bb}Department of Physics and Astronomy, University of Manitoba, MB R3T 2N2, Canada
- ^{bc}Department of Physics, Saitama University, Saitama 338-8570, Japan
- ^{bd}Department of Physics, Chuo University, Tokyo 112-8551, Japan
- ^{be}Science Education, Faculty of Education, Shizuoka University, Shizuoka 422-8529, Japan
- ^{bf}Faculty of Social and Information Sciences, Nihon Fukushi University, Aichi 475-0012, Japan

Contents

1	Background and Previous Studies	5
2	Prospects & Strategy	6
2.1	GRB afterglows	6
2.2	Distant Blazars	7
3	Targets & Feasibility	7
3.1	Origin of Excess of Soft X-ray Absorption	7
3.2	Constrain Progenitor Model and Environment of GRBs by Fe-K Line and Recombination Edge	8
3.3	Soft X-ray Lines from GRB Afterglow	10
3.4	Expected Number of Events of GRB Afterglow by <i>Astro-H</i>	10
3.5	Distant Blazar spectral simulation of absorption features by IGM	11
4	Additional Science — hard X-ray observations of Blazar and GRB Continua	13

1 Background and Previous Studies

In the optical and near IR, deep Hubble and ground based observations has revealed the formation and evolution of galaxies up to $z \sim 8$ (Bouwens et al., 2010) allowing constraints on the star formation rate over the last 13 Gyrs of cosmic time. While the star formation rate is directly connected to the chemical evolution of the universe, one must make assumptions about the initial mass function, the types of supernova that have exploded and the yields of the SN to directly relate star formation to chemical production. Direct measurement of the abundance of the elements at high redshifts is thus critical but has proven to be difficult, except for a few high signal to noise optical observations of the host galaxies of gamma-ray bursts. Somewhat surprisingly present day observations of the high redshift IGM has shown little evidence for chemical evolution.

Based on models of galaxy formation, the relative population of massive stars is thought to increase in the high- z universe and the rate of type Ia supernova is thought to be lower than those of type II. These assumptions can be checked via measurement of the $\text{Fe}_{\text{II}} / \text{Mg}_{\text{II}}$ ratio. However, no clear evidence of chemical evolution in $\text{Fe}_{\text{II}} / \text{Mg}_{\text{II}}$ ratio has been detected and there is a fairly large scatter in this ratio seen in the high redshift universe (De Rosa, 2011).

X-ray observations, in contrast to optical and IR observations, can determine the abundances in massive systems such as clusters and groups of galaxies and, potentially, in the dominant baryonic reservoir at $z < 1$, the hot ionized intergalactic medium. In the last two decades, there has been extensive analysis of the abundances in the hot intra-cluster medium (ICM) at $z < 0.5$, showing little if any evolution; but the data at higher redshifts are rather poor. However, despite of *ASTRO-H*'s high sensitivity compared with the previous X-ray mission, it will require very long observations to measure cluster chemical abundances at high redshifts.

In this white paper we show the possibility of measuring the chemical evolution of the universe beyond $z \sim 1$ utilizing bright background light sources such as Blazars and X-ray afterglows of gamma-ray bursts (GRBs). Since the X-rays are absorbed by primarily K shell electrons, we can measure not only cold neutral gas but also the expected warm-hot intergalactic medium (WHIM) and the hotter ICM with X-ray absorption features. Thus the X-ray spectra will measure not only the local intra-galactic medium around these sources but also the global chemical environments in the high- z universe.

A significant detection of the WHIM has been one of critical observational issues in high energy astrophysics, since it should provide a solution to the “missing baryon problem”. At $z = 0$, the local baryon density calculated from summing up well-observed baryons (viz. stars, neutral atomic gas, molecular gas and X-ray emitting hot gas) is $\Omega \approx 0.0068$ for $H_0 = 70 \text{ km s}^{-1} \text{ Mpc}^{-1}$ (Fukugita et al., 1998), which is much less than the value expected from Big Bang nucleosynthesis, according to the WMAP and Planck observations of the cosmic microwave background and what is seen in the high- z universe. Thus there must be a large amount of, so far, undetected baryons in the local universe consistent with theoretical studies such as that of Cen & Ostriker (2006) whose cosmological hydrodynamic simulations, find that $\sim 50\%$ of all baryons are in the WHIM at $z = 0$. This implies that the majority of the missing baryons are hidden in the warm-hot material. Therefore it is critical to detect it and determine its physical properties. The WHIM is expected to be filamentary, shock-heated IGM created during the formation of large-scale structure. Cen & Ostriker (2006) showed that the mass fraction of WHIM increases from $\sim 10\%$ at $z = 3$ to $\sim 50\%$ at $z = 0$.

For recent decades, several detections of WHIM in the X-ray spectra of blazars have been reported using *Chandra*/LETG or *XMM-Newton*/RGS (Fujimoto et al., 2004; Williams et al., 2006; Takei et al., 2007; Rasmussen et al., 2007, e.g.). Most of these detections either low statistical significance or cannot confirmed with independent observations, except for some exceptions focusing IGM associated with known signpots of superclusters (Buote et al., 2009; Ren et al., 2014). The difficulty in evaluating possible line absorption structures is mainly because one has to search the entire sightline to rule out statistical fluctuations (Kaastra et al., 2006).

By observing the IGM over a wide range of redshifts, *ASTRO-H* might play a crucial role in solving the missing baryon problem. It is believed that the WHIM has so far escaped significant detection because of the lack of a high throughput, high resolution X-ray spectrometers and thus is match to *ASTRO-H*'s capabilities, since it is very difficult for it to be detected at other wavelengths or by low resolution X-ray spectrometers. In addition, the *ASTRO-H*'s high resolution spectroscopy over a wide energy range covering iron features,

would be powerful to identify the WHIM distinguishing from hotter intra-group or intra-cluster medium in the line of sight. Should this search be successful or if sensitive upper limits are obtained, it will be a strong observational constraint on the mass fraction and chemical evolution of WHIM and thus provide strong impacts on cosmological models and star formation histories.

2 Prospects & Strategy

GRB afterglows and Blazars are ideal sources to search for absorption due to distant material thanks to their bright structureless continuum, with no intrinsic spectral features and their high redshift. To determine the chemical composition of the absorbing material in the line of sight, it is crucial to resolve the fine spectral structures of the edges, resonant lines, and emission lines to determine the redshift and their ionization state. It is reasonable to lay a cornerstone in the *performance verification phase* to evaluate following systematic study of chemical evolution in the high- z universe.

The prospects of *scientific results* and the strategy for the *ASTRO-H* early phase observations in this field are:

Investigate the WHIM along the line of sight to well chosen $z \sim 1 - 3$ objects : We propose to employ GRB afterglows and distant Blazars, in order to survey the WHIM in the distant universe, By measuring the redshifts and ionization state of the intervening gas, we may reveal the missing baryons and their properties. The expected range of the redshift of the spectral features will be $1 \lesssim z \lesssim 3$ as discussed in following subsections.

Investigate ISM and ejecta of Hypernovae with emission features in GRB afterglows: In addition to the expected absorption features of the IGM, we can also search for emission features from local dense ISM associated with the GRB and from ejecta in GRBs afterglow emission.

2.1 GRB afterglows

The progenitor of the “long” duration GRB is thought to be due to the core collapse of a massive star (Woosley, 1993). Although the redshift distribution of GRBs ranges up to $z \sim 10$ (Jakobsson et al., 2006), the peaking of the distribution is observed around $z \sim 1$. Since their radiation energy (of the order of 10^{52} erg s^{-1}) is ~ 10 times larger than those of normal core-collapse supernovae, it is widely accepted that the radiation from GRB emissions is produced in highly relativistic jets pointing at the observer. The extreme Lorentz factor of $\gamma \sim 10^3$ requires a rare type of supernovae as the GRB progenitor.

The tightly beamed high intensity intrinsically featureless emission makes the GRB an ideal background light for irradiating intervening matter in the high- z universe. However, somewhat surprisingly, the X-ray spectra of high redshift GRBs show evidence for significant absorption in excess of the Galactic foreground. the origin of this absorption is not well understood. This absorption is often attributed to the gas in the host galaxy, since the majority of long GRBs are associated with the deaths of massive stars and often lie in active star forming regions which are associated with dense gas. If the nature of these star forming regions are similar, the apparent column density of the X-ray absorbing material should (corrected for the redshift of the source) be roughly constant with redshift. However, detailed analysis Campana et al. (2010), Behar et al. (2011), Watson & Jakobsson (2012), and Starling et al. (2013), shows that many high redshift bursts exhibiting high intrinsic absorption beyond that seen in lower redshift objects. Behar et al. (2011) proposed that the X-ray flux from distant objects such as GRB afterglows and distant Blazars inevitably suffers absorption from the IGM in addition to possible absorption in the host galaxies. Following Behar et al. (2011), Starling et al. (2013) recently showed that moderately metal enriched and warm gas with an estimated ionization parameter with $\xi \equiv (L/n_e r^2) \sim 20$ is a viable explanation for the observations of the high redshift high column density X-ray absorption, where the L , n_e , and r are the luminosity, electron number density, and distance of the ionized plasma from the light source. This WHIM like absorber exhibits a relatively *flat* optical depth with redshift in the soft X-ray band which seems to compensate for the expected decrease of optical depth at the observer rest frame. These papers clearly showed that X-ray spectroscopic studies of GRB afterglows are quite promising method to investigate the IGM at high redshift.

However, in the absence of sensitive high resolution spectroscopy, it is impossible to conclusively determine the nature of absorbers and their locations especially for the redshift distributions. The spectral resolution of absorption features is the key to determining their chemical abundance, ionization state and physical origin. This is undoubtedly one of the frontiers for *ASTRO-H* to pioneer.

In addition to the diffuse IGM, the expected dense circumstellar medium (CSM) associated with the GRB progenitor may produce heavy elements atomic lines and/or edges in the afterglow spectrum. So far, the best evidence for such features as been in the Fe-K band. Marginal evidence for iron features has been claimed in several X-ray afterglows (Piro et al., 1999; Yoshida et al., 1999; Piro et al., 2000). They, however, are still controversial, not only due to the limited statistics but also for the rather tight upper limits in other afterglows (Yonetoku et al., 2000).

Almost 100 % of GRBs are followed by the bright X-ray afterglows while only ~ 60 % show the detectable optical counter parts. One of the reason for the lack of optical emission is caused by the absorption in the host galaxies of GRBs. Thus these optically dim bursts should show strong X-ray absorption signatures making X-ray observations of GRB *X-ray* afterglows a serious contender for detailed *ASTRO-H* observations.

We demonstrate the capability to resolve the expected features in the X-ray afterglow in § 3.1 and 3.2.

2.2 Distant Blazars

Blazars are active galactic nuclei in which the photon emission is dominated by a relativistic jet pointing toward observers, and their energy spectra has less intrinsic spectral features. While Blazars are the most luminous AGN, they are not as instantaneously bright as X-ray afterglow of GRBs. But their activities last much longer than GRBs, and we must enable to perform continuous observations with longer exposures. Deep *ASTRO-H* observations of Blazars are promising prospects to search for intergalactic absorption features in their spectra.

Although the intrinsic Blazar spectrum is thought to be a featureless continuum, there were some reports of the detection of absorption spectral features in the X-ray of several Blazars. Using the *Einstein* Observatory, Krolik et al. (1985) first reported line-like absorption features in the soft X-ray spectra of the Blazar PKS 2155–304. Following this discovery, a number of authors have searched for absorption features in Blazar X-ray spectra, and there are several claims of narrow absorption lines originating in the IGM, utilizing the *Chandra* and *XMM-Newton* grating spectrometer observations of low redshift ($z < 0.3$) Blazars(e.g. Nicastro et al., 2005). However the existence of these features are still controversial (Kaastra et al., 2006).

Besides the narrow absorption features, Behar et al. (2011) utilizing CCD data carried out a systematic estimation of the excess absorption in Blazar spectra. With their direct measurement of optical depth toward a large sample of Blazars, they showed that foreground diffuse IGM dominates the absorption in high redshift Blazar spectra as well as in GRB afterglows. This result, together with the claimed line absorption features, hints at the existence of the long sought spectral features from the WHIM. Although the redshift and temperature of the absorber have not been accurately determined, due to the limited energy resolution of the CCD spectrometers, the detection of such features with the high energy resolution and high throughput instruments onboard *ASTRO-H*, will allow the redshift, temperature and chemical abundance of the suggested *intrinsic* absorption to be accurately measured.

3 Targets & Feasibility

3.1 Origin of Excess of Soft X-ray Absorption

As in § 2.1, an excess of absorption in soft X-ray band against to the local Galactic value was reported in several papers e.g. Behar et al. (2011) and Starling et al. (2013). Interestingly, the observed absorption column density continuously increases with the redshift of GRBs, which is inconsistent with the simple scenario that the absorption is mainly due to the host galaxy of GRBs. Therefore, those authors suggest that this excess absorption is due to intergalactic material (IGM). Starling et al. (2013) showed that the absorption is consistent with it being due to an ionized absorber (the WHIM) with a temperature of 10^{5-6} K and ionization parameter

of $\xi = 20$. The estimated excess absorption column density has a mean value of 10^{22} cm^{-2} per unit redshift. Following Starling et al. (2013), we simulated absorption this material using XSTAR with parameters of (gas temperature of 10^5 K , column density of 10^{22} cm^{-2} , and the heavy elemental abundance of 0.2), and placed at a redshift of 0.1 and with the background continuum due to a near and bright GRB afterglow.

A 100ks exposure of a GRB in which we used as inputs the results of 1 for GRB 991216 (as summarized in Table 1) clearly exhibits detections of absorption lines, associated with Fe and oxygen ions around 0.686 and 0.695 keV in observer frame with $4 - 5 \sigma$ significance level. In order to show the sensitivity of the SXI and the SXS to the ionization state of the intervening gas we also show the residuals from an alternative model — single power-law with absorption by a cold-neutral material — in the bottom panel of the figure. In addition to these absorption features, we also simulated emission features reported in Piro et al. (2000) but assumed relatively narrow line case ($\sigma = 10 \text{ eV}$). Detailed discussion on the emission features are described in section 3.2. Such emission line features are clearly detected even for flux level of $10^{-12} \text{ erg cm}^{-2} \text{ s}^{-1}$. Figure 1 right shows the 100 ks observation of the same afterglow. . The possibility of *ASTRO-H* observing such a bright GRB afterglow is discussed in detail in § 3.4.

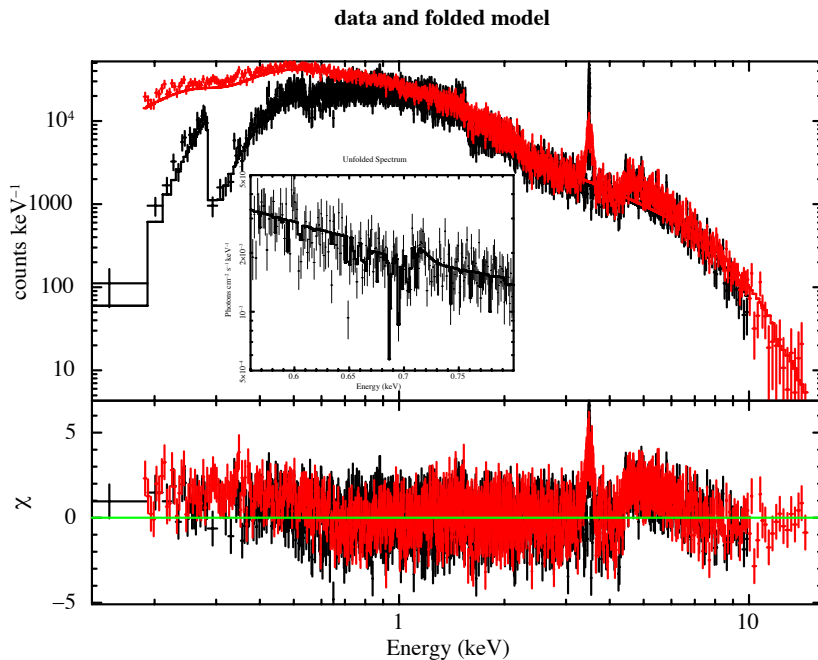


Figure 1: *ASTRO-H* simulation of GRB afterglow spectrum with the warm absorber model. The red points show the SXI and the black the SXS. The assumed intrinsic spectral model is taken from Piro et al. (2000) as summarized Table 1, but we assumed narrow line width of 10 eV. The absorption in soft X-ray band is replaced to warm material using XSTAR. The redshift of warm absorber is set at $z = 0.1$, the gas temperature is 10^5 K , and the absorption column density, N_{H} is 10^{22} cm^{-2} . A 100 ks exposure is assumed to simulate follow-up observation one day after the trigger. The enlarged structure around 0.6 – 0.8 keV, where the most prominent absorption features can be seen are also shown in the inset. Bottom part shows the residuals from single power-law model with absorption from cold materials.

3.2 Constrain Progenitor Model and Environment of GRBs by Fe-K Line and Recombination Edge

Spectral emission features in GRB afterglows are a powerful tool to investigate the circumstellar environment of GRBs. As described in § 2.1, GRB progenitors could be rare type of supernovae. Piro et al. (2000) reported the detection of an Fe-K line feature and a radiative recombination edge in the afterglow spectrum of GRB 991216 at 4σ confidence level. They showed that, utilizing the central energy of Fe-K line and radiative recombination edge, we can determine the redshift of the GRB as well as provide an estimation of the ejecta mass from the

Table 1: *ASTRO-H* simulation of GRB 991216 based on Piro et al. (2000) results

	assumed parameters Piro et al. (2000)
N_{H}^a	$0.35 (\pm 0.15) \times 10^{22} \text{ cm}^2$
photon index	$2.2 (\pm 0.2)$
Edge Energy	$4.4 (\pm 0.5) \text{ keV}$
I_{edge}^b	$3.8 (\pm 2.0) \times 10^{-5} \text{ ph cm}^{-2} \text{ s}^{-1}$
Line Energy	$3.49 (\pm 0.06) \text{ keV}$
I_{line}^b	$3.2 (\pm 0.8)$
$\text{Flux}_{2-10\text{keV}}^c$	$2.3 \times 10^{-12} \text{ erg cm}^{-2} \text{ s}^{-1}$

supernova.

In order to examine the feasibility, of detecting a similar set of spectral features, we simulated the Piro et al. (2000) et al data, assuming a power-law with Fe-K line and recombination edge and parameters. Yonetoku et al. (2000) estimated an upper limit of Fe-K line equivalent width (EW) using ASCA data of GRB 990123 and set it to be 100 eV. Accordingly, here we assumed the EW of 50 eV.

Measurement of the line width provides crucial information for understanding the physics of the ejecta of the GRB progenitor. Piro et al. (2000) claimed a line width $\sigma \sim 200$ eV, but the observational evidence for the width of Fe-K line is not strong due to the energy resolution of the CCD data. The high resolving power of Fe-K line of SXS is much more sensitive than previous instruments for detecting weak narrow Fe-K lines. In Figure 2, we show the results of simulating Fe-K line emission with the SXS based on the spectra of GRB 991216. A weak Fe-K line is detectable by SXS at 5.3σ for 5 eV width and 4.8σ for 10 eV width for a nominal GRB spectrum. Such a feature is not detectable with CCD spectral resolution.

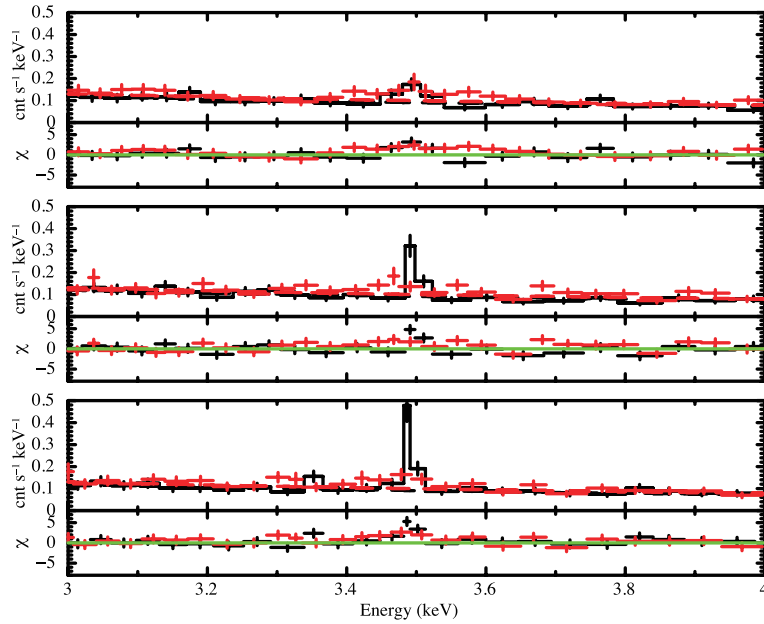


Figure 2: *ASTRO-H* simulation of weak Fe-K line features for various intrinsic line widths. Each panel contains simulated 10 ks spectrum with models (power-law+Fe-K line) and its residuals from single power-law model. We assumed weak Fe-K lines with equivalent width of $\text{EW}=50\text{eV}$ but assumed bright afterglow spectrum with $F_{2-10 \text{ keV}} = 10^{-11} \text{ erg s}^{-1} \text{ cm}^{-2}$. We used various intrinsic line width $\sigma = 30$ eV (top), 10 eV (middle), and 5 eV (bottom).

3.3 Soft X-ray Lines from GRB Afterglow

In addition to the iron features, emission lines from other light elements are important in probing the environment of the progenitor of GRBs. There have been a few claimed detections of emission lines due to Mg, Si, S, Ar, and Ca in some GRB spectra (Reeves et al., 2002; Watson et al., 2003). However these results have not been confirmed in recent *Swift* data (Hurkett et al., 2008). Accurate and significant detection and measurement of the soft X-ray lines with *ASTRO-H* SXS/SXI, is needed to confirm the existence of such features and their use as indicators of chemical evolution in the high- z universe.

We examine the feasibility of detecting the soft X-ray lines with *ASTRO-H*. In these simulations, we calculated the SXS/SXI spectra assuming the reported spectral parameters but doubled the X-ray flux. Since these ISM origin features might be illuminated for a short time, we assumed the exposure time of 10 ks in this simulation. As we can see in the figure, the soft X-ray line features are clearly visible by *ASTRO-H* observation with $\sim 4\sigma$ significance. In this spectral simulation, we assume a line width of 5 eV, since no significant line broadening was reported in the previous observation.

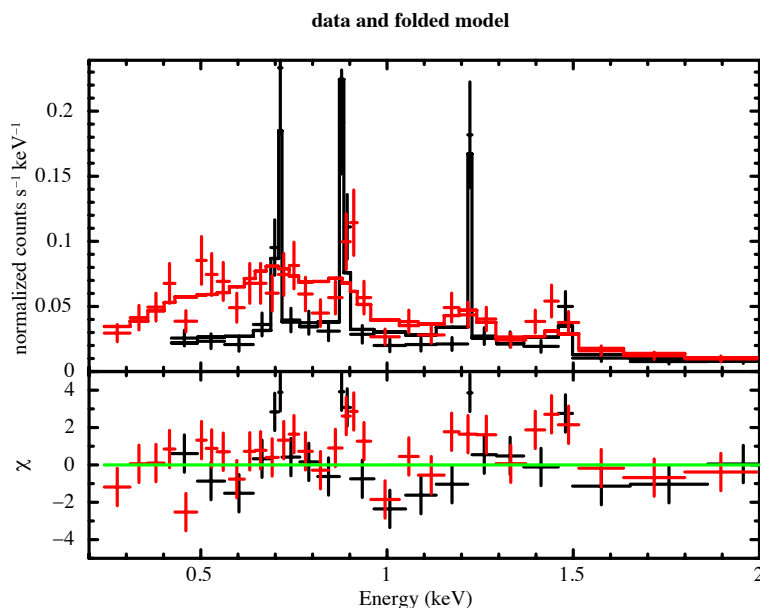


Figure 3: Simulated spectrum of afterglow spectrum of GRB 011211 by *ASTRO-H* SXS (black) and SXI (red), assuming 10 ks of exposure time. Fitted spectral models are also plotted with the solid line. The assumed spectral model was taken from Reeves et al. (2003) but 2 times brighter than previous paper. Bottom panel shows the residuals from single power-law model.

3.4 Expected Number of Events of GRB Afterglow by *Astro-H*

As we showed in previous sections, *ASTRO-H* has a capability of detecting any spectral features such as Fe-K lines, recombination edge, other lines from light metals, and of course absorption by warm intervening materials. In this section, we estimate the expected number of GRBs in which *ASTRO-H* can detect these spectral features. For this estimation, we calculate the luminosity function of X-ray afterglow based on *Swift*/XRT data base which is publicly available in the web site¹.

First, we fit every XRT light curve in the 6-year data base with a simple power-law function of time from the GRB trigger time. We then summarized each afterglow flux of time in “the cumulative luminosity function” as we showed in Figure 4. Finally, we compared the flux level of simulated spectra in the § 3.1 and 3.2 with the estimated luminosity function (Figure 4). According to the simulations as previously shown, in the case of Fe-K line emission and recombination edge, the flux level of 2.3×10^{-12} erg cm⁻² s⁻¹ are required to constrain

¹http://www.swift.ac.uk/xrt_curves

the iron spectral features (in case of GRB 991216, 37 hours after the GRB trigger. The expected event rate is about 3.3 events per year. On the other hand, in the case of our simulation for detection capability of weak Fe-K line, we assumed very bright afterglow with the flux level of $\sim 10^{-11}$ erg cm $^{-2}$ s $^{-1}$. Such flux level at late times is rare with ~ 1 event per year 10 hours after the trigger and 0.3 event per year for 30 hours after the trigger.

In the case to observe the soft X-ray lines, the simulated flux is roughly about 10^{-12} erg cm $^{-2}$ s $^{-1}$ level at 11 hours after the GRB trigger the expected event rate is about 16 events per year. In conclusion, we reasonably expect *ASTRO-H* to be able to observe soft X-ray emission lines from GRB afterglows with an event rate of a few per year, even if it takes one day to slew the spacecraft. But we need to slew within 10 hours after GRB trigger, to detect Fe-K line and edge features with event rate of at least one event per year. A follow-up within 10 hours is possible indeed, since *ASTRO-H* has a slew speed of over $180^\circ/100$ minutes. However, a dedicated operation team for the quick follow-up operation is required as the *Suzaku* GRB follow-up team which succeeded carried out four times of quick follow-up observations within a few hours. At this moment, *ASTRO-H* team has not decided to organize the quick follow-up observation team.

Table 2 summarizes feasibility of GRB observation by *ASTRO-H*.

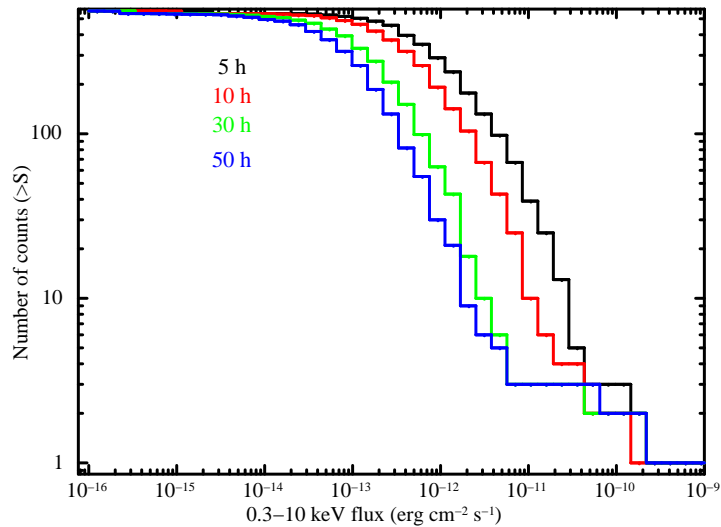


Figure 4: Estimated luminosity functions of GRB afterglow based on 6-years *Swift*/XRT data base. Different colors show the function corresponds to the different observation start time after GRB trigger (black:5 hour, red:10 hours, green:30 hours, and blue:50 hours, respectively). Horizontal and vertical axis is 0.3–10 keV flux in erg cm $^{-2}$ s $^{-1}$ and cumulative number of events, respectively.

Table 2: Summary of expected number of GRB events for various flux level and observation start time

Flux level	event rate per year
	50 hours / 30 hours (~ 1 day) / 10 hours (\sim half day)
10^{-11} erg cm $^{-2}$ s $^{-1}$	0.5 / 0.5 / 1
10^{-12} erg cm $^{-2}$ s $^{-1}$	3 / 10 / 33

3.5 Distant Blazar spectral simulation of absorption features by IGM

Based on their redshift and flux, we have selected four Blazars among the object exhibiting significant excess absorption listed in Table 1 of Behar et al. (2011). Each of four has a 2 – 10 keV flux brighter than 1×10^{-11} erg cm $^{-2}$ s $^{-1}$ and redshift higher than 2 as summarized in Table 3. In this section, we show the simulated spectrum and the results of evolution, utilizing the same XSTAR based WHIM model as employed for GRB afterglows in § 3.1 for the representative Blazar RBS 315, at a redshift of $z = 2.69$.

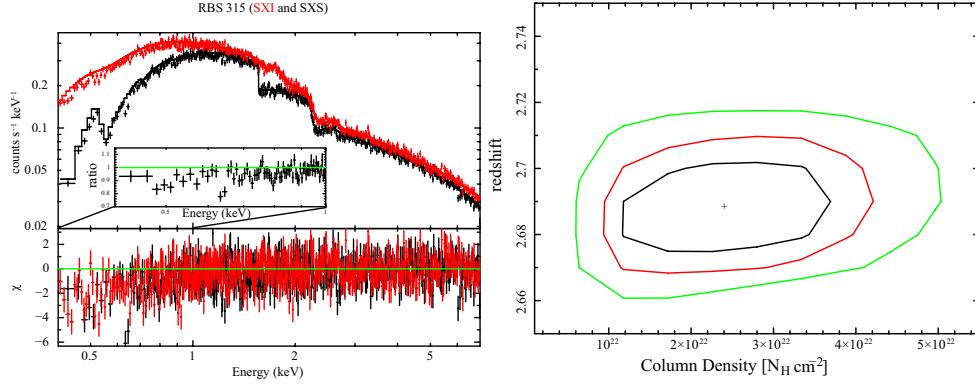


Figure 5: Simulated spectrum of the Blazar RBS 315 by *ASTRO-H/SXS* (black) and *SXI* (red) according to the result by Behar et al. (2011) and a confidence contours to evaluate redshift of the *intrinsic* absorber. WHIM (temperature of 10^6 K, 0.2 solar abundance, column density $N_{\text{H}} = 2.9 \times 10^{22} \text{ cm}^{-2}$) absorber at the source rest frame ($z = 2.69$) is assumed. The simulated spectrum in the left is shown in crosses, and the model from which the WHIM component is removed is indicated with histogram. The WHIM originated spectral features are clearly detected as shown in the inset data to model ratios in the energy range from 0.4 to 1 keV. Residuals are in the lower panel. In the right, we show the confidence contours to demonstrate the expected accuracy with a 300 ks exposure. Each contour denotes 68%, 90%, or 99% level confidence.

Table 3: Spectral parameters of the Target Blazars (Behar et al., 2011)

target name	redshift	$N_{\text{H}}^{\text{Gal},a}$	$N_{\text{H}}^{z,b}$	flux ^c	reference
PKS 2126 – 158	3.366	4.92	1.80	1.10	Fiore et al. (2003)
RBS 315	2.690	9.26	2.90	1.08	Tavecchio et al. (2007)
PKS 2149 – 306	2.345	1.61	0.08	1.00	Bianchin et al. (2009)
4C 71.07	2.172	2.85	0.09	1.40	Malizia et al. (2000)

a: Galactic column density in the unit of $10^{20} \text{ H cm}^{-2}$
b: Intrinsic column density in the unit of $10^{22} \text{ H cm}^{-2}$
c: Observed 2–10 keV flux in the unit of $10^{-11} \text{ erg cm}^{-2} \text{ s}^{-1}$

We show the *ASTRO-H* capability in determining the redshift of the possible absorber in Figure 5. All the simulated spectra shown here assumes the exposure time of 300 ks. Thanks to the excellent energy resolution of the *SXS* crucial for determining the absorption edge energy together with the large effective area for the *SXI* to determine the optical depth, we see that *ASTRO-H* will be able to resolve the absorption line structure to determine the redshift with X-ray spectrum.

In Figure 6, we show that the *SXS* has a capability to measure the temperature of the warm-hot plasmas. The signature of the excess absorption is clearly seen in the data to model ratios, where we removed the intrinsic WHIM absorption model from the model denoted with histogram in Figure 6. In the ratios, we see clear absorption lines due to: $\text{Si}_{\text{VII-XI}}$ at 0.48 keV (1.8 keV at rest frame), $\text{S}_{\text{VIII-XIII}}$ at 0.64 keV (2.4 keV at rest frame), and $\text{Ar}_{\text{X-XII}}$ at 0.81 keV (3.0 keV at rest frame), as well as we see in the inset indicated with energy at the source (WHIM) rest frame. In addition, the difference of temperature of WHIM is seen in the lowest energy bin in the ratios. We also show the confidence contours for the two different temperature WHIM. In the right panel of Figure 6, we clearly see that *ASTRO-H/SXS* determines the WHIM temperature with reasonable accuracy.

We assumed the WHIM at the same redshift frame with the source and demonstrate that *SXS* with *SXI* are able to determine the column density and the temperature. Then we simulated the WHIM at various redshift frame from $z = 0$ to $z = 2.5$ to investigate expected significance of each spectral features of elements. Figure 7 shows the signal to noise ratios of absorption lines of Fe, Mg, Si, S, or Ar of the WHIM at each redshifts. The assumed WHIM temperature is 10^5 K and other parameters were the same as described above. All elements but Ar are to be detected with the significance of $S/N > 4$ at any redshift between 0 and 2.5. Moreover WHIM in

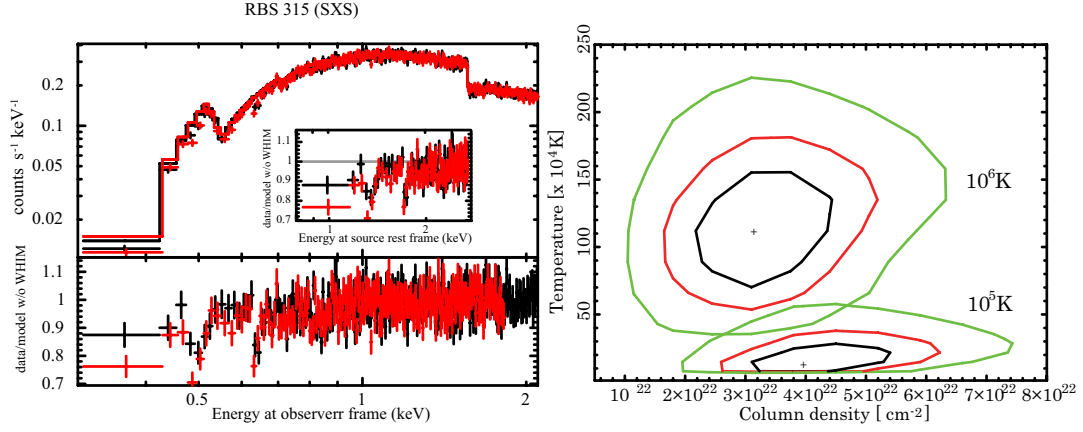


Figure 6: (left) The *ASTRO-H*/SXS simulated spectrum of the Blazar RBS 315 (utilizing the model of Behar et al. (2011)). The reported intrinsic absorption column was replaced with WHIM and Galactic absorption. Both absorption models are calculated with XSTAR. The assumed temperatures of WHIM are 10^5 K (red) and 10^6 K (black). Other parameters employed here are the same as those used in § 3.1 except that the WHIM absorber is redshifted ($z = 2.69$) to demonstrate the capability determining the redshift of absorber. The histogram shows the model without the intrinsic absorption but only with the Galactic absorption to demonstrate the expected intrinsic absorption features in data to model ratios in the bottom panel. The inset shows the same features in ratios with energy in the WHIM rest frame. The ionization features are clearly shown in the energy band below 1.0 keV. (right) Confidence contours to demonstrate that SXS will clearly distinguish the assumed two different temperatures. The WHIM model generated with XSTAR is employed to evaluate each intrinsic absorption feature that we assumed in the left simulations.

the range of $0 < z < 1$, in which large portion of the WHIM are expected (section 1), the expected significance fairly exceeds 5 or more.

Since the intrinsic Blazar exhibits featureless spectrum, every bright distant Blazar is a potential target to search for the intervening WHIM and/or other absorption materials. Many of these sources have strong flaring episodes and are monitored by *MAXI* and *Swift* and thus are candidates for ToO observations. In addition to those Blazars listed in table 3, a number of Blazars in the redshift range from $z = 1 - 3$ have a high X-ray flux $> 10^{-11}$ erg cm $^{-2}$ s $^{-1}$ in hard X-ray band (Tüller et al., 2010; Ghisellini et al., 2011). For example, we could add Blazars Swift J1656.3–3302, [HB89] 0212+735, or [HB89] 0836+710 for their expected high flux in the SXS band. However, neither Swift J1656.3–3302 sitting behind the Galactic center region nor 0836+710 exhibiting rather low intrinsic absorption are suitable for the early phase target to explore the WHIM. The rest 0212+735 could be added the target list to be monitored, although the uncertainty of the reported intrinsic absorption are fairly large in comparison with RBS 315 discussed above.

4 Additional Science — hard X-ray observations of Blazar and GRB Continua

As intensive follow up observations with *Swift* have revealed, most of GRB afterglows experience a series of decay phases, such as a steep decay, a shallow decay, a normal decay and a *jet decay* phase after the jet break (Nousek et al., 2006). Assuming that follow-up observation start $\sim 30 - 60$ hours after the burst, as discussed in § 3.4, it should be possible to observe the *jet decay* phase in hard X-rays. Since the jet break is thought to be caused by deceleration of a shocked shell in the GRB jet, such measurements will scan the shock shell from small to large radius as the beaming factor decreases after the jet break via measuring the *curvature* of the continuum using a wide band spectrum as a function of time. In other words, observing the jet break is a scanning observation of the shock front, since the beaming factor of the emission region decreases dramatically during the jet break decays. This will provide an excellent chance to resolve the GRB jet internal structure by utilizing the wide band *ASTRO-H* X-ray data.

While the *Suzaku*/HXD has observed four GRB afterglows a few hours after the GRB prompt emissions, it did not accurately measure the hard X-ray spectra because of its limited sensitivity. The HXI, however, with a two orders of magnitude higher sensitivity, will be able to observe the hard X-ray spectrum as well as the soft X-ray instruments (SXI/SXS), as far as the follow up observation by *ASTRO-H* is carried out.

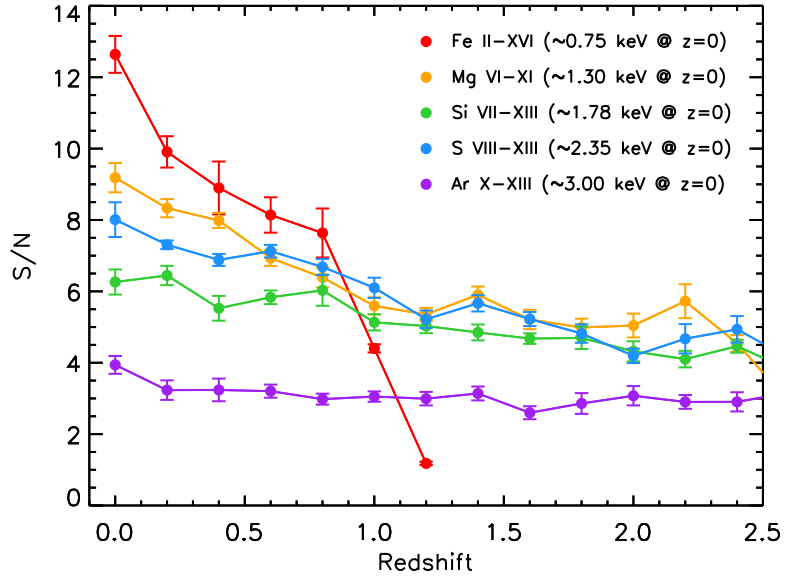


Figure 7: The expected significance of each element absorption line of WHIM at $z = 0 - 2.5$ with the 300 ks observation of the *ASTRO-H* SXS/SXI. The Blazar RBS 315 whose X-ray flux and spectral parameters are described in table 3 is assumed to be the WHIM irradiating source. The assumed parameters of WHIM are described in § 3.1 while the temperature employed in this simulation is 10^5 K.

The HXI and SGD data will precisely determine the continuum shape of the afterglow, which increases the accuracy of column density measurement discussed above.

References

- Behar, E., Dado, S., Dar, D., Laor, A. 2011, *ApJ*, 734, 26
- Bianchin, V. et al. 2009, *A&A*, 496, 423
- Boettcher, M., Dermer, C.D.D., Crider A.W., Liang, E.D. 1999, *A&A*, 343, 111
- Bouwens, R. J. et al. 2010, *ApJ*, 709, L133
- Buote, E., Zappacosta, L., Fang, T. et al. 2009, *ApJ*, 695, 1351
- Campana, S., Thöne, C.C., de Ugarte Postigo, A., et al. 2010, *MNRAS*, 402, 2429
- Campana, S., et al., 2012, *MNRAS*, 410, 1611
- Cen, R. & Ostriker, J. P., 2006, *ApJ*, 650, 560
- Cucchiara, A., Prochaska, J. X., Zhu, G., et al. 2013, *ApJ*, 773, 82
- Chugai, N.N., et al. 2004, *MNRAS*, 352, 1213
- Fujimoto, R., Takei, R., Tamura, T. et al. 2004, *PASJ*, 56, L29
- Fiore, F., et al., 2003, *A&A*, 409, 57
- Fukugita, M., et al. 1998, *ApJ*, 503, 518
- De Rossa et al. 2011, *ApJ*, 739, 56
- Ghisellini et al. 2011, *MNRAS*, 411, 901
- Hurkett et al. 2008, *ApJ* 679, 587
- Jacobsson, P. et al. 2006, *A&A*, 447, 897
- Kaastra, J. S., Werner, N., den Herder, J. W. A., et al. 2006, *ApJ*, 652, 189
- Krolik, J.H., Kallman, T.R., Fabian, A.C., Rees, M.J., 1985, *ApJ*, 295, 104
- Malizia, A., et al. 2000, *ApJ*, 531, 641
- Mészáros, P., Rees, M.J. 1998, *MNRAS*, 299, L10
- Nicastro, F., Mathur, S., Elvis, M. et al. 2005, *ApJ* 629, 700
- Nousek, J. A., Kouveliotou, C., Grupe, D., et al. 2006, *ApJ*, 642, 388
- Perna, R. & Loeb, A. 1998, *ApJ*, 501, 467
- Piro, L. et al. 2000, *Science*, 290, 955
- Piro, L., et al. 1999, *ApJ*, 514, L73
- Rafelski, M., Wolfe, A. M., Prochaska, J. X. et al. 2012, *ApJ*, 755, 89
- Rasmussen, A. P., Kahn, S. M., Paerels, F. et al. 2007, *ApJ*, 656, 129
- Reeves, J. N. et al. 2002, *Nature*, 416, 512
- Reeves, J. N. et al. 2003, *A&A*, 403, 463
- Ren, B., Fang, T., & Buote, D. A. 2014, *ApJ*, 782, L6
- Savaglio, S. 2012, *Astron. Nachr.*, 333, 480
- Savaglio, S. 2009, *Proc. IAU Symp.*, 265, 119
- Schlegel, E.M. 1990, *MNRAS*, 244, 269
- Shimizu, T., Masai, K., Koyama, K. 2012, *PASJ*, 64, 24
- Starling, R.L.C., Willingale, R., Tanvir, N.R., et al. 2013, *MNRAS*, 431, 3159
- Takei, Y., Henry, J. P., Finaguenov, A., et al. 2007, *ApJ* 655, 831
- Tavecchio, F., et al. 2007, *ApJ*, 665, 980
- Tüller, J. et al. 2010, *ApJS*, 186, 378
- Tominaga, N. et al. 2007, *ApJ*, 660, 516
- Watson, D., et al. 2003, *ApJ*, 595, L29
- Watson, D., & Jacobsson, P., 2012, *ApJ*, 754, 89
- Williams, R. J., Mathur, S., Nicastro, F., & Elvis, M., 2006, *ApJ*, 642, L95
- Woosley, S.E. 1993, *ApJ*, 403, 273
- Yoshida, A., et al. 1999, *Proc. of "Gamma-ray bursts in the afterglow era"* (eds. Frontera & Piro), (*A&AS*, 138), 433
- Yonetoku, D., et al. 2000, *PASJ*, 52, 509-625